

Article

Elimination of Pharmaceutical Compounds from Aqueous Solution through Novel Functionalized Pitch-Based Porous Adsorbents: Kinetic, Isotherm, Thermodynamic Studies and Mechanism Analysis

Qilin Yang ¹, Hongwei Zhao ^{1,2,*} , Qi Peng ¹, Guang Chen ¹, Jiali Liu ¹, Xinxiu Cao ^{1,2} , Shaohui Xiong ^{1,2} , Gen Li ^{1,2} and Qingquan Liu ^{1,2,*} 

¹ School of Material Science and Engineering, Hunan University of Science and Technology, Xiangtan 411201, China; a3346529088@163.com (Q.Y.); pengqi408@126.com (Q.P.); cghnust@163.com (G.C.); 17373487964@163.com (J.L.); xxcao@hnust.edu.cn (X.C.); xiongshaohui@hnust.edu.cn (S.X.); genkevinli@hnust.edu.cn (G.L.)

² Hunan Provincial Key Laboratory of Advanced Materials for New Energy Storage and Conversion, Hunan University of Science and Technology, Xiangtan 411201, China

* Correspondence: hwzhao@hnust.edu.cn (H.Z.); qqliu@hnust.edu.cn (Q.L.)

Abstract: The long-term presence of PPCPs in the aqueous environment poses a potentially significant threat to human life and physical health and the safety of the water environment. In our previous work, we investigated low-cost pitch-based HCP adsorbents with an excellent adsorption capacity and magnetic responsiveness through a simple one-step Friedel–Crafts reaction. In this work, we further investigated the adsorption behavior of the prepared pitch-based adsorbents onto three PPCP molecules (DFS, AMP, and antipyrine) in detail. The maximum adsorption capacity of P-MPHCP for DFS was 444.93 mg g⁻¹. The adsorption equilibrium and kinetic processes were well described through the Langmuir model and the proposed secondary kinetic model. The negative changes in Gibbs free energy and enthalpy reflected that the adsorption of HCPs onto PPCPs was a spontaneous exothermic process. The recoverability results showed that the adsorption of MPHCP and P-MPHCP onto DFS remained above 95% after 10 adsorption–desorption cycles. The present work further demonstrates that these pitch-based adsorbents can be used for multiple applications, which have a very extensive practical application prospect.

Keywords: HCP adsorbents; pitch-based; magnetic; PPCPs



Citation: Yang, Q.; Zhao, H.; Peng, Q.; Chen, G.; Liu, J.; Cao, X.; Xiong, S.; Li, G.; Liu, Q. Elimination of Pharmaceutical Compounds from Aqueous Solution through Novel Functionalized Pitch-Based Porous Adsorbents: Kinetic, Isotherm, Thermodynamic Studies and Mechanism Analysis. *Molecules* **2024**, *29*, 463. <https://doi.org/10.3390/molecules29020463>

Academic Editors: Dimitrios Giannakoudakis and Angelo Fenti

Received: 1 January 2024

Revised: 13 January 2024

Accepted: 15 January 2024

Published: 17 January 2024



Copyright: © 2024 by the authors. Licensee MDPI, Basel, Switzerland. This article is an open access article distributed under the terms and conditions of the Creative Commons Attribution (CC BY) license (<https://creativecommons.org/licenses/by/4.0/>).

1. Introduction

Global economic and population growth is currently leading to the troubling reality of the pervasive contamination of freshwater ecosystems. Pharmaceuticals and personal care products (PPCPs), along with other trace organic pollutants, have become pervasive sources of pollution [1,2]. PPCPs are available in a wide range of categories including antibiotics, anti-inflammatory drugs, β -blockers, anticonvulsants, lipid modulators, etc. [3,4]. According to World Health Organization (WHO) statistics, the global consumption of pharmaceuticals has been estimated at 100,000 tons per year [5]. PPCPs can re-enter the environment through various pathways [6–9]. Despite undergoing conventional wastewater treatment, significant PPCP residues can persist in effluent, with certain pharmaceuticals like diclofenac exhibiting removal rates as low as 10% [10–12]. Alarmingly, these remnants of novel antibiotic products can contribute to the development of drug-resistant bacteria, thereby escalating public health concerns.

Traditional wastewater treatment methods like activated sludge, membrane filtration, and photodegradation suffer from inherent shortcomings, notably secondary pollution, high costs, and limited efficiency [13–16]. For instance, the cost of biological treatment

ranges from 0.17 to 0.53 €/m³, but it achieves only a 55% removal rate for PPCPs. Photocatalysis comes at a steep cost of 10.36 €/m³, but it does achieve high removal rates. Hybrid technology, with a cost of 0.17–0.75 \$/m³, may necessitate pre-treatment for specific wastewater samples; however, the integration process demands more processing units, leading to increased energy consumption [17]. As an alternative, adsorption has proven to be effective as it is simple to operate, less likely to cause secondary pollution, and the adsorbent can be regenerated. However, traditional adsorption materials have restricted pores and poor chemical stability [18]. To address this challenge, organic porous materials are being developed as new, effective adsorbent materials to meet current demands.

Porous organic polymers (POPs) represent a promising breakthrough in adsorbent materials for the removal of PPCPs from wastewater [19,20]. These materials are crafted by covalently linking organic monomers, thereby resulting in a customizable network structure featuring high specific surface areas, exceptional chemical and thermal stability, and a uniform pore configuration [21]. Hypercrosslinked polymers have displayed remarkable efficiency in the elimination of waterborne contaminants including PPCPs. Ravi et al. synthesized two new phosphate-based POPs and evaluated their effectiveness in adsorbing PPCPs [22]. The results showed that the maximum adsorption of P-POP-2 onto caffeine, diclofenac, and carbamazepine was 301, 217, and 248 mg g⁻¹, respectively. Gan et al. pioneered the creation of oxygen-rich hypercrosslinked polymers through a tandem of continuous Friedel–Crafts reactions [23]. This innovative approach significantly enhanced the adsorption of aniline onto these synthesized polymers, showcasing a remarkable maximum capacity of 178.4 mg g⁻¹ at 303 K. Hao et al. successfully synthesized a covalent organic framework (COF-SO₃H) that was functionalized with sulfonic acid (-SO₃H) groups for the effective removal of PPCPs [24]. It was shown that COF-SO₃H exhibited a strong affinity for all 13 PPCPs studied, with especially noteworthy properties in the adsorption of diclofenac. COF-SO₃H achieved a maximum adsorption capacity of 770 mg g⁻¹. Organic porous polymers hold immense promise for PPCPs adsorption applications. Hence, the pursuit of cost-effective, highly efficient, and readily producible POP adsorbents carries substantial practical importance.

Pitch poses potential hazards due to its composition containing pyridine, benzene, and naphthalene, which can lead to severe harm through skin contact, inhalation, or extended environmental exposure. Consequently, the environmentally responsible use of pitch, particularly its transformation into an adsorbent for water treatment, represents a highly desirable application [25]. Yang and collaborators have showcased the remarkable versatility of pitch-based hypercrosslinked polymers (PHCPs) as carbon precursors for crafting nitrogen-doped layered porous carbon materials (N-PHCP-900), notably enhancing oxygen reduction reaction (ORR) performance. N-PHCP-900 exhibited exceptional ORR performance in alkaline electrolytes, outperforming both commercial Pt/C and most non-precious metal electrocatalysts [26]. This demonstrates that the removal of PPCPs through hyper-crosslinked modified pitch-based polymers is a feasible approach, especially considering the cost-effectiveness and the simple procedure involved [27–29].

In our previous work, we designed and synthesized functionalized Fe₃O₄ magnetic nanoparticles (Fe₃O₄@3-phenylglutaric acid NPs) to both magnetize and enhance the functionality of pitch-based hypercrosslinked polymers. Meanwhile, by utilizing Friedel–Crafts reaction method, three cost-effective, pitch-based, high-performance adsorbents (PHCP, MPHCP, and P-MPHCP) were prepared [30]. As shown in Figure 1, pure pitch was used to synthesize PHCP. Through the combination of pitch and Fe₃O₄@3-phenylglutaric acid NPs, MPHCP, a magnetic pitch-based HCP featuring carboxyl functionalization, was synthesized. To enable a more precise comparison of the effects of the two different functional groups, P-MPHCP was synthesized using pitch, Fe₃O₄@3-phenylglutaric acid NPs, and phenol. This was undertaken while considering the intricate composition of pitch with the potential presence of phenolic hydroxyl groups. The isotherms, kinetics, thermodynamics, and recoverability of these pitch-based HCPs for the adsorption of three PPCPs (diclofenac (DFS), 4-acetylaminophenol (AMP), and antipyrine) were investigated

in detail. The mechanism of PPCP adsorption was elucidated through infrared spectra and XPS analysis of the samples before and after adsorption.

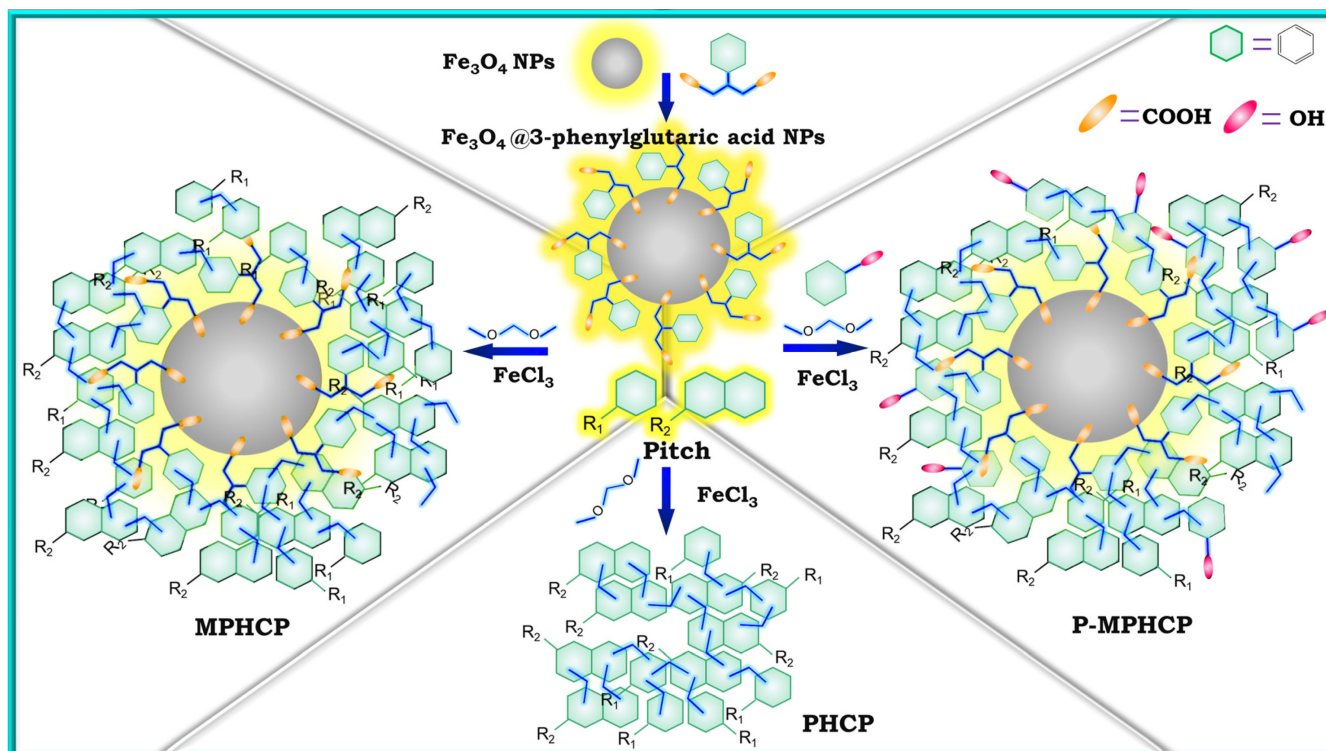


Figure 1. The synthetic scheme of $\text{Fe}_3\text{O}_4@3\text{-phenylglutaric acid NPs}$, PHCP, MPHCP, and P-MPHCP.

2. Results and Discussions

2.1. pH-Dependent Adsorption Behaviors of Pitch-Based HCPs

There is a statistically significant effect of the pH level on the adsorption process, mainly in terms of the surface charge and morphology of the adsorbent [31]. Exploring the optimal pH conditions for the adsorption of various PPCP yields crucial insights. These insights are essential for designing efficient and environmentally friendly treatment methods for wastewater containing these contaminants. The equilibrium concentrations of the samples were assessed with a standard curve, and the linear Beer–Lambert relationship was given through the calibration plot of absorbance versus the concentration, as shown in Figure S1. Figure 2 demonstrates the effect of pitch-based HCPs on the adsorption efficiency (%) of three PPCPs (DFS, AMP, and antipyrine) at different pH levels (4–10). The results showed a significant increase in the adsorption efficiency with an increasing pH level, reaching a maximum level of efficiency at the pH levels of 5, 6, and 7 for DFS, AMP, and antipyrine, respectively. In the case of a relatively low pH level (<4), the lower adsorption rate of the adsorbents is attributed to the fact that the protonated forms of all PPCPs may limit interaction with the surface of the protonated adsorbent. With a higher pH level, the deprotonated forms of PPCPs may weaken interaction with the surface sites of the adsorbent due to the increase in the concentration of free hydroxyl ions in the aqueous solution, thereby leading to a decrease in the adsorption performance [32]. Therefore, further adsorption studies were carried out at the optimal pH levels of 5, 6, and 7 for DFS, AMP, and antipyrine, respectively.

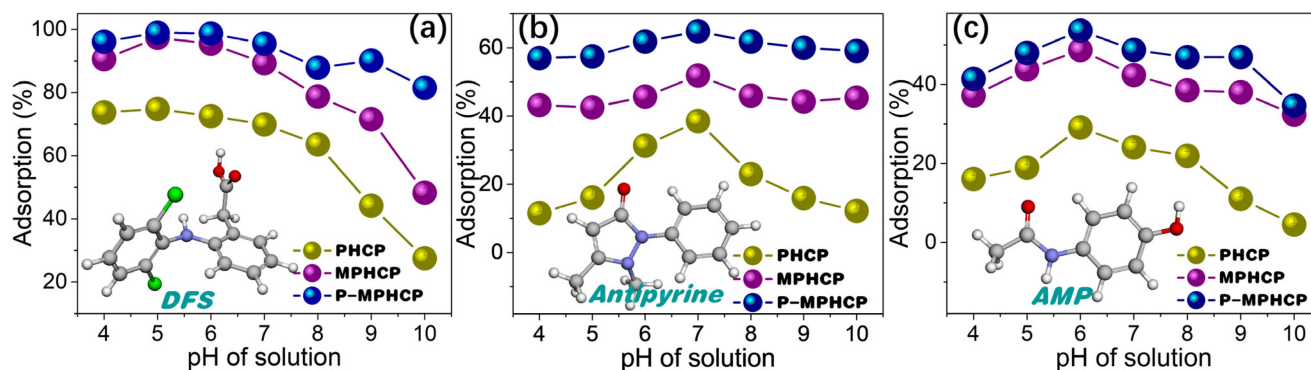


Figure 2. pH-dependent adsorption capacities of the pitch-based HCP adsorbents to DFS (a), antipyrine (b), and AMP (c).

2.2. Adsorption Kinetics

To understand the adsorption rate, the effect of the contact time of pitch-based HCPs onto PPCPs at the optimal pH level on their adsorption performance was investigated. As shown in Figure 3, the adsorption process of PPCPs through the adsorbent first exhibited a rapid increase and then tended to an adsorption equilibrium of around 80 min. Among the three adsorbents, P-MPHCP showed the strongest adsorption capacity for PPCPs; the order of adsorption capacity was P-MPHCP > MPHCP > PHCP, and the adsorption efficiencies of P-MPHCP for DFS, AMP, and antipyrine were 85.58, 40.88, and 54.21%, respectively. In addition, P-MPHCP, MPHCP, and PHCP all showed more a prominent adsorption capacity for DFS, with adsorption efficiencies of 85.58, 64.92, and 35.02%, respectively. The specific surface areas of PHCP, MPHCP, and P-MPHCP in BET tests were 531, 483, and 468 $\text{m}^2 \text{g}^{-1}$, respectively. The introduction of functional groups, such as carboxyl or phenolic hydroxyl groups, plays a crucial role in enhancing the adsorption capacity of MPHCP and P-MPHCP for PPCPs. This leads to PHCPs having a larger specific surface area but a lower adsorption capacity. Consequently, it can be deduced that the incorporation of functional groups, such as carboxyl or phenolic hydroxyl, significantly improves the adsorption capacity of adsorbents onto PPCPs.

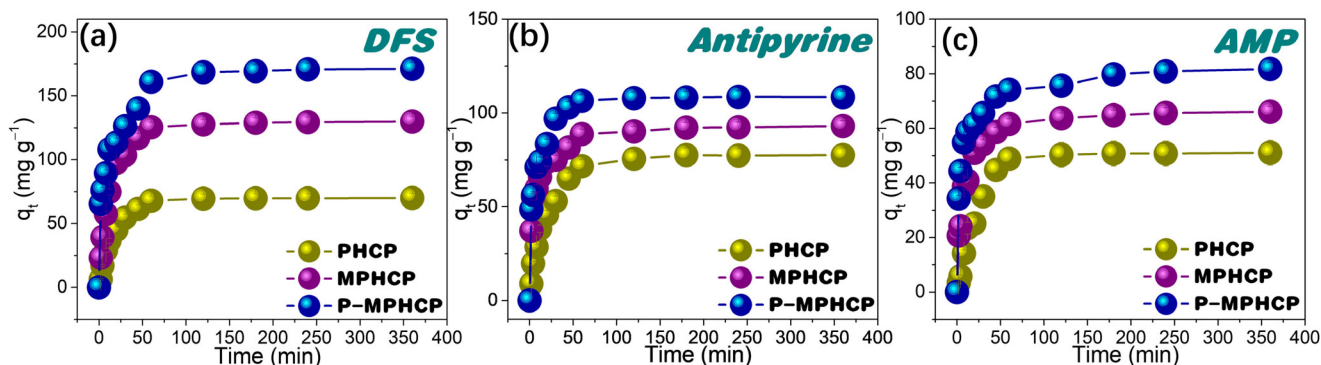


Figure 3. Adsorption kinetic results for pitch-based HCP adsorbents onto DFS (a), antipyrine (b), and AMP (c).

For a more comprehensive assessment of the adsorption kinetics, the adsorption data were subjected to a thorough analysis using pseudo-first-order and pseudo-second-order kinetic models [33,34], as described by Equations (1) and (2), respectively.

$$\text{Pseudo - first order : } \ln (q_e - q_t) = \ln q_e - K_1 t \quad (1)$$

$$\text{Pseudo - second order : } \frac{t}{q_t} = \frac{t}{q_e} + \frac{1}{q_e^2 K_2} \quad (2)$$

Herein, q_t (mg g^{-1}) represents the adsorption capacity at time t (minutes), while q_e (mg g^{-1}) represents the adsorption capacity at equilibrium. The parameters K_1 (min^{-1}) and K_2 ($\text{g mg}^{-1} \text{min}^{-1}$) stand for the rate constants associated with pseudo-first-order and pseudo-second-order adsorption, respectively. The proposed first-order and proposed second-order adsorption kinetics of HCPs on PPCPs are shown in Figure 4, and the parameter fitting results are shown in Table 1. In contrast, the pseudo-second order kinetic model, as depicted in Figure 4 and detailed in Table 1, exhibits an exceptionally precise fit for the PHCPs, yielding R^2 values ranging from 0.9959 to 0.9999. The results demonstrated that the fitted results of the pseudo-second-order kinetic model were greatly superior to the pseudo-first-order kinetic model. P-MPHCP and MPHCP exhibit significantly higher adsorption capacities for PPCPs compared with PHCP. This is primarily due to the increased availability of adsorption sites facilitated through the carboxyl/phenolic hydroxyl groups. As a result, the adsorption mechanism governing the interaction between HCPs and PPCPs was primarily chemisorption-based, with the functional groups contributing to the augmentation of the available adsorption sites.

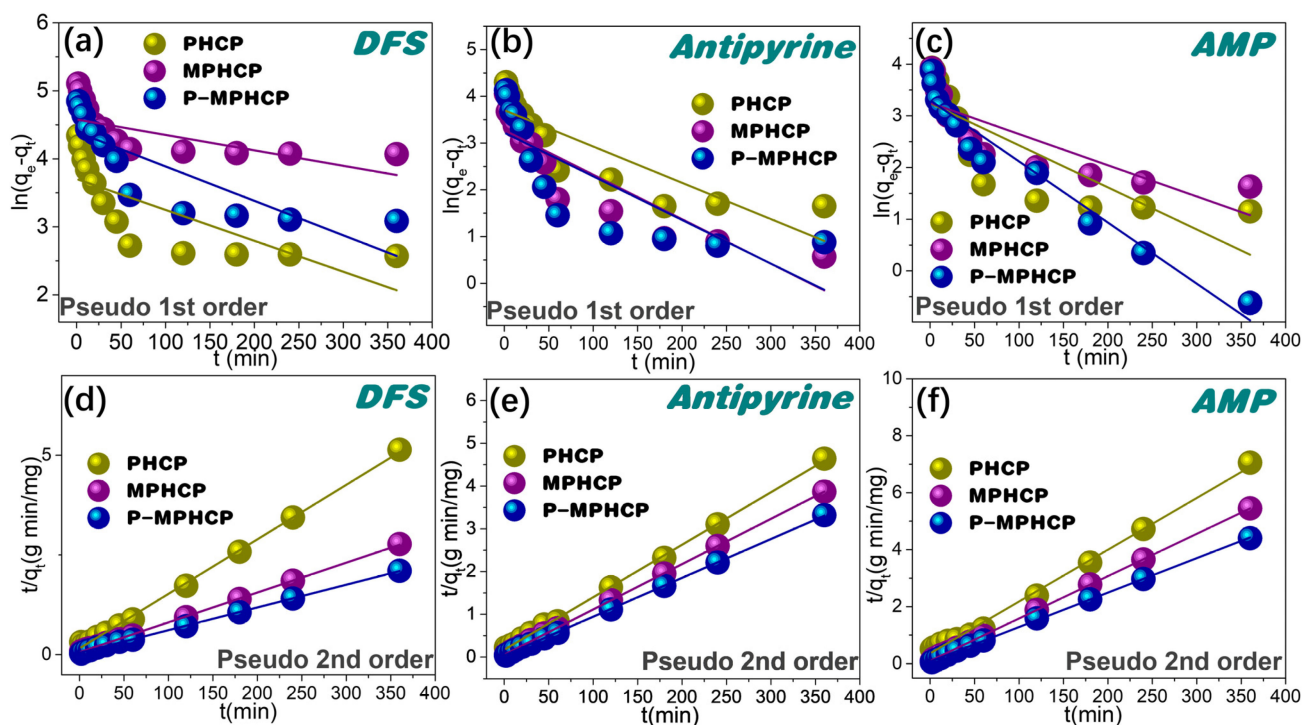


Figure 4. Adsorption kinetics for pitch-based HCP adsorbents onto PPCPs fitted with the pseudo-first order kinetic models of (a–c) and the pseudo-second order kinetic models of (d–f).

Table 1. Adsorption kinetics of DFS, AMP, and antipyrine onto HCPs.

Sample	PPCP	Pseudo-First Order Kinetic Model			Pseudo-Second Order Kinetic Model		
		q_e (cal) (mg g^{-1})	K_1 (min^{-1})	R^2	q_e (cal) (mg g^{-1})	K_2 ($\text{g mg}^{-1} \text{min}^{-1}$)	R^2
PHCP	DFS	40.62	0.0045	0.5767	73.09	0.0012	0.9985
	AMP	25.64	0.0081	0.6665	54.97	0.00092	0.9959
	Antipyrine	40.58	0.0077	0.7569	81.36	0.00088	0.9993
MPHCP	DFS	106.80	0.0024	0.5128	133.51	0.00093	0.9997
	AMP	25.82	0.0060	0.6910	67.24	0.0023	0.9999
	Antipyrine	26.51	0.0095	0.8066	94.25	0.0021	0.9998
P-MPHCP	DFS	81.09	0.0050	0.6963	175.43	0.00076	0.9994
	AMP	27.13	0.011	0.9471	82.64	0.0021	0.9996
	Antipyrine	25.09	0.009	0.6517	110.01	0.0023	0.9998

The potential for intraparticle diffusion was investigated through the utilization of the Weber–Morris model, represented through the following Equation:

$$q_t = k_{IP}t^{0.5} + C \quad (3)$$

In this equation, k_{IP} represents the intraparticle diffusion rate constant ($\text{mg g}^{-1} \text{min}^{0.5}$), while C is the intercept resulting from the plot of q_t against $t_{0.5}$. This plot should yield a straight line with a slope equal to k_{IP} when the adsorption mechanism adheres to the intraparticle diffusion process (as shown in Figure 5). The intraparticle diffusion model for PPCPs can be divided into three distinct steps as follows: (1) an immediate ascension phase driven by interactions between PPCPs and the functional groups; (2) the process of intraparticle diffusion within the porous structure; and (3) reaching an equilibrium stage [35]. It is worth highlighting that the linear fitting plots did not start from the point of origin, suggesting that intraparticle diffusion is not the sole limiting factor of the rate [36]. The effectiveness of the adsorption of PPCPs might be influenced by a combination of factors including the size of the PPCP molecules and the distribution of the adsorbent's pore structure.

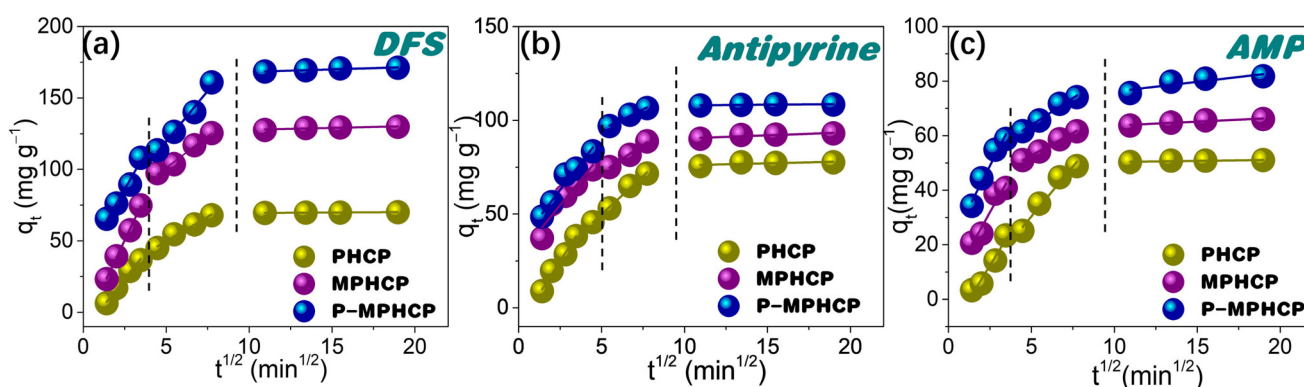


Figure 5. Weber–Morris intraparticle diffusion model for PHCP, MPHCP, and P-MPHCP toward DFS (a), antipyrine (b), and AMP (c) at initial concentrations of 200 mg L^{-1} .

2.3. Effect of Initial Concentration

To investigate the effect of the initial concentration on the adsorption capacity of the adsorbents, isothermal equilibrium adsorption experiments were conducted at the optimal pH solution. These experiments covered a range of initial PPCP concentrations from 100 to 350 mg L^{-1} . Figure 6, Figures S2 and S3, depict the influence of the initial PPCP concentration on the adsorption capacity at temperatures of 25 , 35 , and $45 \text{ }^\circ\text{C}$, respectively. Comparing the adsorption properties of the three pitch-based adsorbents onto PPCPs, P-MPHCP showed the most exceptional adsorption capacity. This was followed by MPHCP and finally PHCP, which was neither magnetized nor modified and showed the weakest adsorption capacity. For instance, the adsorption efficiency of DFS in solution was significantly high for all pitch-based HCPs ($\geq 94\%$) at concentrations ranging from 100 to 200 mg L^{-1} . At lower solution concentrations, the introduction of phenolic hydroxyl groups did not significantly affect the adsorption. This could be attributed to the availability of more adsorption sites than needed. When the initial concentration was set at 350 mg L^{-1} , the maximum adsorption capacities for DFS onto PHCP, MPHCP, and P-MPHCP were found to be 173.20 , 253.38 , and 316.78 mg g^{-1} , respectively. It is indicated that the introduction of the carboxyl and phenolic hydroxyl groups after magnetic functionalization does indeed enhance the adsorption capacity of the adsorbent onto PPCPs. Moreover, all three adsorbents showed a consistent trend in the adsorption capacity to PPCPs along the order of $\text{DFS} > \text{antipyrine} > \text{AMP}$.

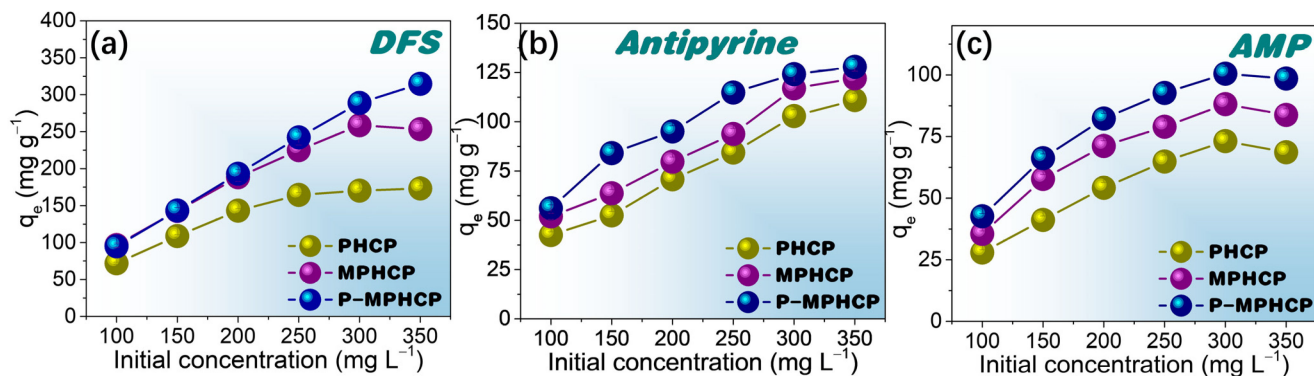


Figure 6. Isotherm adsorption capacity for pitch-based HCP adsorbents onto DFS (a), antipyrine (b), and AMP (c) with different initial concentrations at 25 °C.

2.4. Adsorption Isotherms

The adsorption efficiency of the adsorbents was investigated using adsorption isotherms to evaluate the adsorption of the adsorbents, the correlation between equilibrium adsorption and equilibrium concentration, and the mutual interaction between the adsorbent and the adsorbent surface. Equations (4)–(6) for the Freundlich, Langmuir, and Dubinin–Radushkevich (*D–R*) models are represented as follows [37–39]:

$$\text{Langmuir : } \frac{C_e}{q_e} = \frac{C_e}{q_{max}} + \frac{1}{q_{max} K_L} \quad (4)$$

$$\text{Freundlich : } \ln q_e = \ln K + \frac{\ln C_e}{n} \quad (5)$$

$$\text{Dubinin–Radushkevich (D–R) : } \ln q_e = \ln q_{D-R} - B\varepsilon^2, \quad \varepsilon = RT \ln \left(1 + \frac{1}{C_e} \right), \quad E_a = \frac{1}{\sqrt{2B}} \quad (6)$$

In these equations, q_e represents the adsorption capacity (mg g^{-1}), C_e is the equilibrium concentration (mg L^{-1}), q_{max} stands for the maximum adsorption capacity (mg g^{-1}), K_L is the binding strength constant (L mg^{-1}), while K and n are constants denoting adsorption capacity and intensity. B is the adsorption energy constant ($\text{mol}^2 \text{kJ}^{-2}$), ε signifies the Polanyi potential, R represents the gas constant ($8.314 \text{ J (mol K)}^{-1}$), T indicates the absolute temperature (K), and E_a represents the mean energy of adsorption (kJ mol^{-1}).

Freundlich-, Langmuir-, and *D–R*-fitted isotherms for the adsorption of PPCPs at 25 °C are shown in Figure 7a–i. Two fitted models for 35 and 45 °C are shown in Figures S4 and S5. The model Langmuir and Freundlich model fitting parameters are shown in Table 2; for almost all isotherms, the Langmuir model is more suitable than the Freundlich model. Therefore, the adsorption behavior of pitch-based HCPs onto PPCPs is analogous to that of monolayer adsorption. In addition, the Langmuir isotherm fit from Table 2 shows that the R_L values are between 0 and 1, indicating that the adsorption process is spontaneous [40]. The parameters obtained from the Freundlich isotherms in Table 2 show that the values of $1/n$ are in the range of 0.1–0.5, indicating that the pitch-based HCPs have good adsorption performance on PPCPs. Based on the Langmuir model, the P-MPHCP's monolayer adsorption capacities were 444.93, 160.80, and 211.12 mg g^{-1} for DFS, AMP, and antipyrine, respectively. The Langmuir model assumes a uniform surface with consistent activation energy for adsorption, making it suitable for describing adsorption on homogeneous surfaces. On the other hand, the Freundlich model is better suited for surfaces that exhibit a high degree of heterogeneity. Analyzing the results presented in Table 2, Tables S1 and S2, it becomes evident that the Langmuir model provides a more accurate fit compared with the other two isotherm models. This suggests that the adsorption process likely involves predominantly monolayer adsorption, primarily driven through a site-to-site adsorption mechanism. Additionally, the E_a values obtained from the *D–R* isotherm model offer

insights into the type of adsorption. The calculated E_a values fall within the range of 8 to 16 kJ mol⁻¹, indicating that the adsorption is primarily characterized by chemisorption.

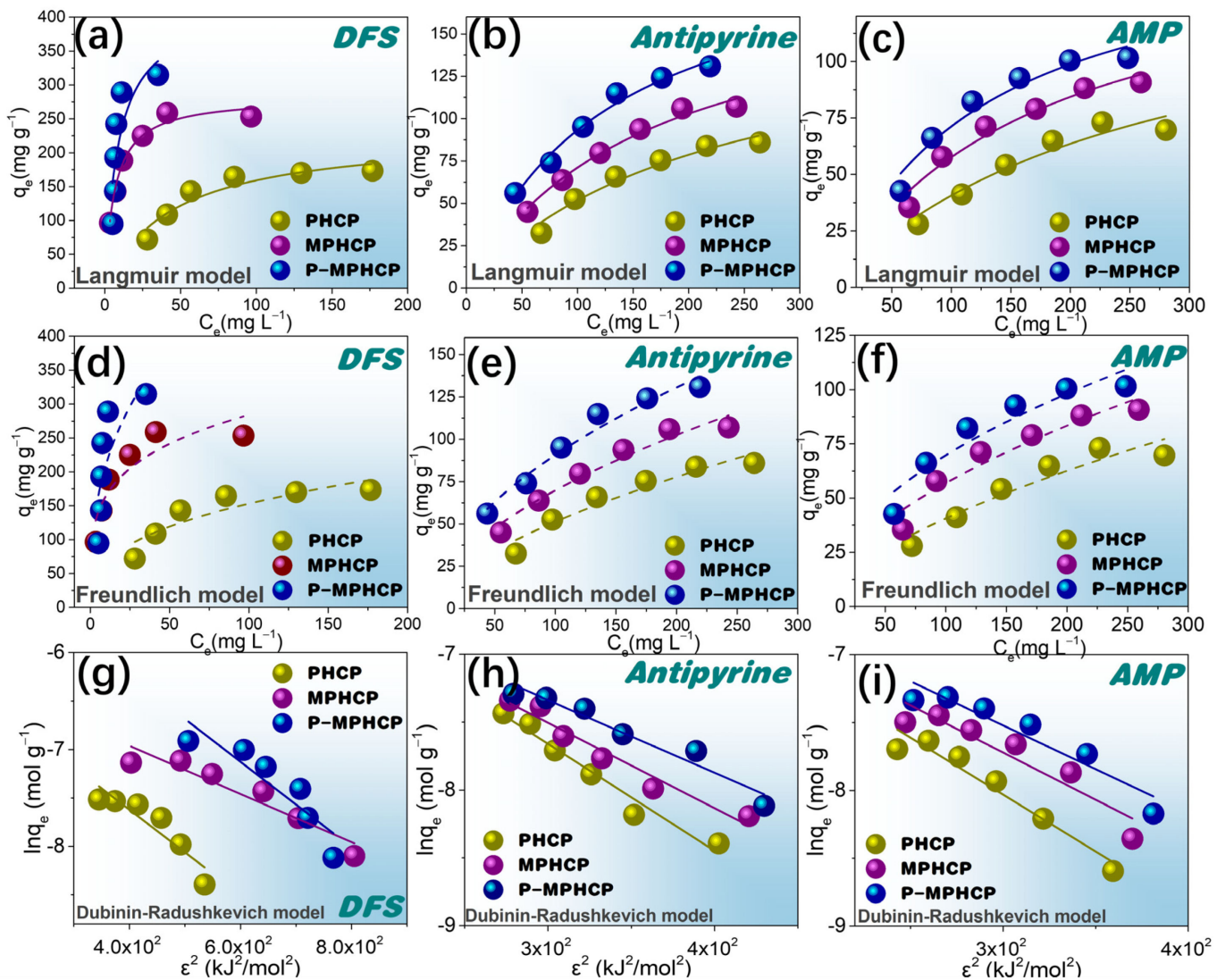


Figure 7. Langmuir (a–c), Freundlich (d–f), and D–R (g–i) isotherms for the adsorption of pitch-based HCP adsorbents onto DFS, antipyrine, and AMP at 25 °C.

Table 2. Correlation coefficient and isotherm parameters for the adsorption of pitch-based HCP adsorbents at 25 °C.

Sample	PPCP	Langmuir Isotherm			Freundlich Isotherm			Dubinin–Redushkevich Isotherm			
		q_{max}	K_L	R^2	n	K_F	R^2	q_{DR}	B	E_a	R^2
PHCP	DFS	229.30	0.022	0.9054	2.76	28.89	0.8088	0.0028	0.0044	10.66	0.8407
	AMP	145.32	0.0038	0.9356	1.60	2.30	0.9031	0.0040	0.0084	7.72	0.9420
	Antipyrine	163.70	0.0046	0.9626	1.66	3.25	0.9322	0.0050	0.0079	7.96	0.9666
MPHCP	DFS	282.56	0.15	0.9804	4.24	95.94	0.8375	0.0026	0.0025	14.17	0.9005
	AMP	156.80	0.0058	0.9567	1.81	4.48	0.9222	0.0036	0.0070	8.47	0.8802
	Antipyrine	186.01	0.0061	0.9823	1.80	5.45	0.9573	0.0036	0.0063	8.91	0.9525
P-MPHCP	DFS	444.93	0.092	0.9116	2.30	75.06	0.8165	0.0053	0.0080	7.93	0.9195
	AMP	180.89	0.0052	0.9327	1.72	4.23	0.8958	0.0034	0.0057	9.36	0.9885
	Antipyrine	223.62	0.0058	0.9763	1.72	5.57	0.9579	0.0114	0.0044	10.64	0.8216

2.5. Adsorption Thermodynamics

The adsorption isotherm is affected by temperature, and the van't Hoff equation can be used to define the thermodynamic parameters. The effect of temperature is illustrated through the adsorption of PPCPs at 25, 35, and 45 °C, as shown in Table 3. The data indicate that temperature is detrimental to adsorption, and the higher the temperature the smaller the q_e . Moreover, these results were fitted with the Langmuir and Freundlich models, as shown in Figures S4 and S5, and the fitted parameters are listed in Tables S1 and S2. The thermodynamic values of adsorption such as the enthalpy of adsorption ΔH (kJ mol⁻¹), free energy of adsorption ΔG (kJ mol⁻¹), and entropy of adsorption ΔS (J (mol K)⁻¹) can be calculated through the following Equations (7)–(9) [41–43]:

$$\ln K_L = -\frac{\Delta H}{RT} + \ln K_0 \quad (7)$$

$$\Delta G = -RT \ln K_L \quad (8)$$

$$\Delta S = \frac{\Delta H - \Delta G}{T} \quad (9)$$

Table 3. Thermodynamic parameters for PPCP adsorption onto pitch-based HCP adsorbents.

Sample	PPCP	T (°C)	ΔH° (kJ mol ⁻¹)	ΔS° (J mol ⁻¹)	ΔG° (kJ mol ⁻¹)
PHCP	DCF	25	−9.6507	−71.52	−7.7365
		35			−7.3997
		45			−6.3060
	AMP	25	−3.4053	7.12	−3.3673
		35			−4.0867
		45			−3.5096
	Antipyrine	25	−3.65246	−1.89	−3.7936
		35			−3.2094
		45			−3.7557
MPHCP	DCF	25	−12.3543	1.69	−12.543
		35			−4.9310
		45			−6.0347
	AMP	25	−2.5186	65.05	−11.753
		35			−5.3425
		45			−5.2577
	Antipyrine	25	−3.31449	45.84	−11.213
		35			−4.1104
		45			−3.7338
P-MPHCP	DCF	25	−10.1730	49.67	−12.577
		35			−6.3273
		45			−4.1057
	AMP	25	−4.3284	30.98	−12.914
		35			−5.6500
		45			−4.3574
	Antipyrine	25	−5.2217	4.31	−12.747
		35			−5.7737
		45			−5.2127

Here, K_L represents the adsorption equilibrium constant with units of L mol⁻¹, R is the universal gas constant at 8.314 J (mol K)⁻¹, T signifies the absolute temperature in Kelvin (K), and K_0 is a constant.

Table 3 reveals that the ΔH value is negative, indicating an exothermic adsorption process of surface HCPs onto PPCPs. The thermodynamic parameters, as derived from

Equations (9)–(11), are presented in Table 3. Notably, all the ΔG values are observed to be negative across all temperatures during the PPCP adsorption process. This observation indicates that the removal of PPCPs is a spontaneous and thermodynamically favorable process. Furthermore, it is observed that as the operating temperature increases the value of ΔG also increases. This suggests that higher operating temperatures do not promote an enhancement in adsorption capacity. In addition, the negative values of ΔH indicate that the adsorption of PPCPs is indeed an exothermic reaction.

2.6. Recyclability of Pitch-Based HCPs

The regeneration of pitch-based HCPs was evaluated to verify their recoverability and stability. Adsorption–regeneration cycle experiments were performed through efficient separation with an applied magnetic field, and the experimental conditions of adsorption were kept constant during each cycle. Figure 8 shows ten adsorption/desorption cycle experiments of pitch-based HCPs onto PPCPs. The experimental results showed that the adsorption efficiency of adsorbents decreased slightly (<5%) after the first five repeated cycles. Finally, it was observed that the adsorption efficiency of MPHCP was 88.4, 74.01, and 80.05% for DFS, AMP, and antipyrine, respectively; the adsorption efficiency of P-MPHCP was 90.9, 82.19, and 84.54% for DFS, AMP, and antipyrine, respectively. Hence, the prepared pitch-based HCP adsorbents exhibit excellent reusability, high adsorption capacity, ease of separation, and hold significant promise for efficiently removing PPCPs from wastewater.

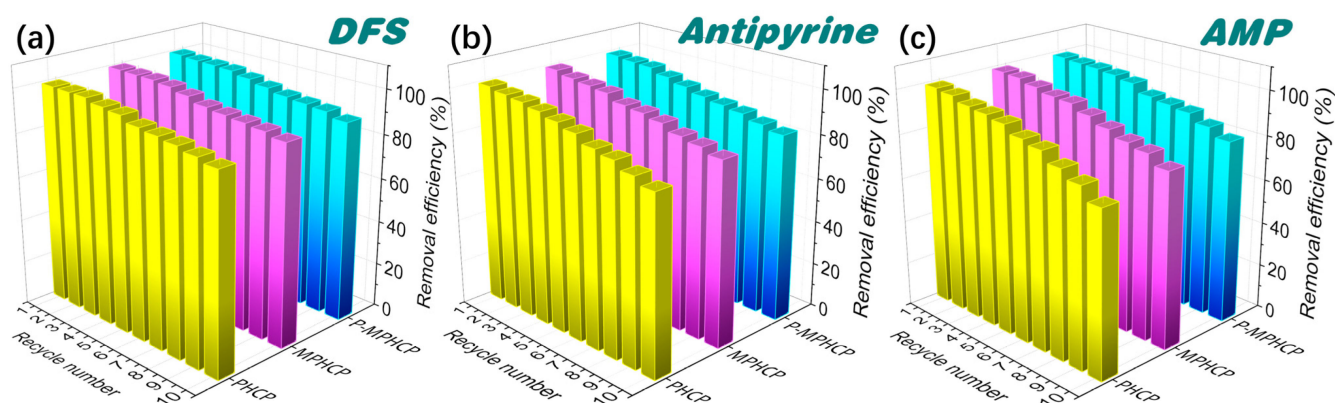


Figure 8. Cycled adsorption/desorption runs of PHCP, MPHCP, and P-MPHCP for DFS (a), antipyrine (b), and AMP (c).

2.7. Adsorption Mechanism

As shown in Figure 9a, P-MPHCP demonstrated a notably higher adsorption capacity when compared with the data provided in Table S3, highlighting its superior performance. Understanding the adsorption mechanism holds paramount importance, serving to not only clarify the fundamental principles of adsorption but also to pave the way for potential commercial applications.

2.7.1. Pore Structure

While highly porous adsorbents with extensive specific surface areas are typically expected to enhance adsorption capacity, our experiments revealed an interesting outcome. Despite possessing a highly specific surface area, PHCP exhibited a relatively lower adsorption capacity compared with P-MPHCP. This suggests that factors beyond specific surface area play a significant role in pharmaceutical compound adsorption. Specialized interactions between the adsorbent and pharmaceutical compounds are particularly noteworthy for influencing the adsorption process [44].

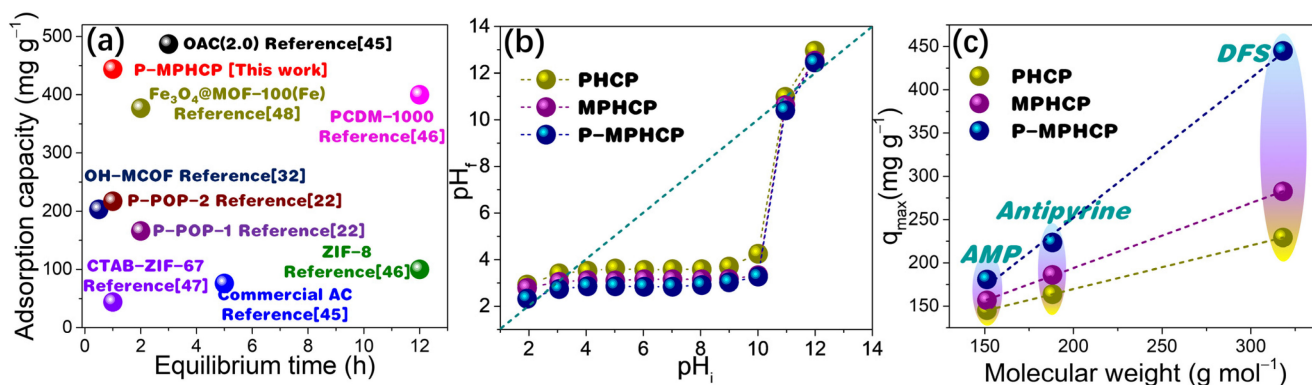


Figure 9. Comparisons of equilibrium time vs. adsorption capacity for PPCP adsorption in P-MPHCP and previously reported benchmark materials (a) [22,32,45–48]; determination of the pH_{pzc} of pitch-based HCP adsorbents through the pH drift method (b); adsorption quantity relationship with the molecular weight of PPCPs (c).

2.7.2. Electrostatic Interaction

Electrostatic interactions between adsorbate molecules and adsorbent surfaces can occur due to the presence of ionizable functional groups [49]. The solution's pH level plays a crucial role as it impacts both the surface charge of the adsorbent and the extent of PPCP dissociation [50]. As shown in Figure 9b, the points of zero charge (pH_{pzc}) for pitch-based HCP adsorbents measured through the pH drift method are 3.46, 3.06, and 2.53, respectively. Thus, the surface of the pitch-based adsorbents was negatively charged (pH > pH_{pzc}) when adsorption studies were performed at the optimal pH levels of 5, 7, and 6 for DFS, AMP, and antipyrine, respectively. For pharmaceutical molecules, at pH > pK_a, the pharmaceutical molecules are negatively charged and at pH < pK_a, the pharmaceutical molecules are in a neutral form [51]. Hence, under optimal pH conditions, both the pitch-based adsorbents and DFS (with a pK_a of 4.15) exhibit negative charges, whereas antipyrine (with a pK_a of 1.4) also carries a negative charge, and AMP (with a pK_a of 9.38) remains neutral (Figure S6) [52,53]. Consequently, it can be inferred that electrostatic interactions do not play a dominant role in the adsorption of PPCPs onto pitch-based adsorbents.

2.7.3. Molecular Dimension

As displayed in Figure 9c the molecular weight of PPCPs had a strong positive correlation with the gravimetric capture capacity (mg g⁻¹) of pitch-based adsorbents. A consistent relationship between the molecular weight of pharmaceutical compounds and their adsorption capacities onto porous polymer adsorbents was observed for pitch-based adsorbents [22]. Notably, larger molecules such as DFS exhibited higher q_m values compared with smaller molecules like AMP. This indicates that the number of adsorption sites distributed in the pores of the pitch-based adsorbent should be approximately identical. This is particularly relevant in the case of adsorption sites fully occupied by several PPCP molecules after adsorption saturation [54]. Meanwhile, the adsorption interaction mechanism of the pitch-based adsorbent for several PPCP molecules should be analogous, and consequently the adsorption capacity exhibits a high degree of correlation with the molecular weight. Therefore, for the three PPCPs, it is possible that some co-occurring adsorption interactions, such as the formation of the hydrogen-bonding interaction as well as the π-π* dispersion interaction, may play a major contribution in the adsorption process.

2.7.4. Hydrogen-Bonding Interaction

The hydroxyl groups on the surface of the pitch-based adsorbent act as hydrogen donors. In turn, the oxygen or nitrogen atoms in the PPCPs serve as hydrogen acceptors, resulting in a dipole–dipole hydrogen-bonding interaction. Another type of hydrogen bonding, known as Yoshida-type, occurs between the hydroxyl groups of adsorbents and

the aromatic rings of the PPCPs [55]. As depicted in Figure 10, similar stretching bands were observed at 760, 830, and 1500 cm^{-1} for both PPCPs and PPCP-adsorbed MPHCPs, confirming the presence of adsorbed PPCPs in pitch-based adsorbents. It becomes evident that following the adsorption process, the band corresponding to hydroxyl groups (at 3434 cm^{-1}) exhibited a reduced intensity. This reduction confirms the presence of hydrogen-bonding interactions between the PPCPs and the pitch-based adsorbents. Notably, the decrease in intensity was more pronounced for P-MPHCP compared with MPHCP, possibly due to OH interactions [56].

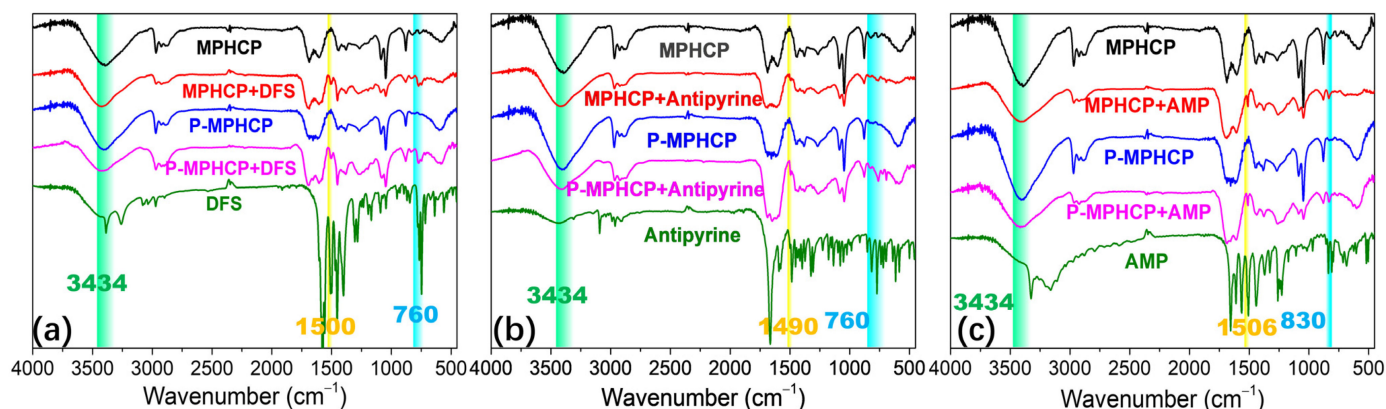


Figure 10. FTIR spectra of adsorbents before and after DFS (a), antipyrine (b), and AMP (c) adsorption.

As shown in Figure 11e–h, analysis of the O1s spectrum was deconvoluted into four peaks for MPHCP corresponding to C=O (531.62 eV), C–OH (532.44 eV), C–O (533.21 eV), and C(O)O (533.96 eV) [57]. After adsorption, there was a notable reduction in the atomic fractions of C–OH in the O1s spectra of MPHCP, amounting to a decrease of approximately 9–11%. This observation suggests that dipole–dipole hydrogen bonding played a significant role in the adsorption of PPCPs. For P-MPHCP, after the introduction of a significant number of phenolic groups, the positions and atomic fractions of several oxygen atoms before and after adsorption were approximately unchanged, which was mainly attributable to Yahida-type H bonding with the benzene ring.

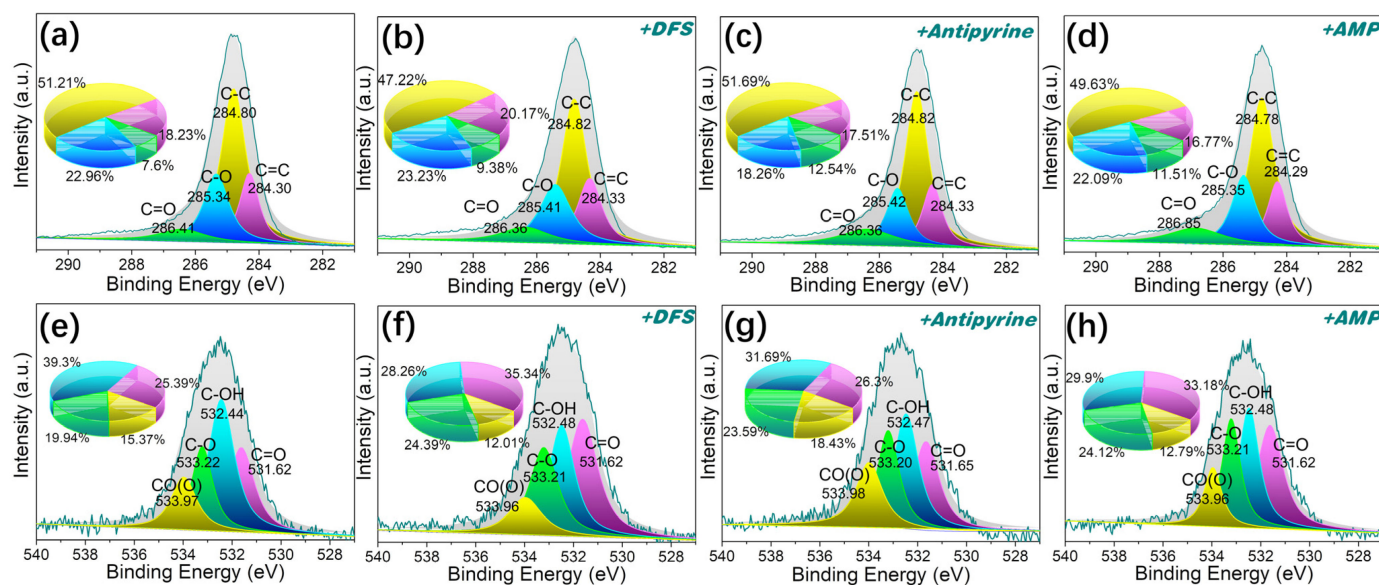


Figure 11. The XPS spectra of C1s (a–d) and O1s (e–h) for MPHCP before and after PPCP adsorption.

2.7.5. π - π^* Dispersion Interaction

Given the abundance of aromatic structures in pitches, it is plausible that π - π^* dispersion interactions between these aromatics in the adsorbent and pharmaceutical compounds play a role in their adsorption. It has been reported that π - π^* interactions tend to exert a dominant influence [58]. This interaction occurs between the aromatic rings of the pharmaceutical compounds and the aromatic structure in pitch-based adsorbents. P-MPHCP showed a much better adsorption performance compared with MPHCP. These interactions are a permanent feature in aromatic compounds and gain strength as the number of aromatic rings in polymers and PPCP molecules increases. Furthermore, as shown in Figure 12, the intensities and areas of the peaks representing the π - π^* interactions increased after DFS capture. Analysis of the XPS data revealed that the C1s spectrum could be sorted into five distinct peaks at approximately 284.3 (C=C), 284.8 (C-C), 285.3 (C-O), 286.4 (C=O), and 288.1 eV (π - π^* interactions), respectively [59,60]. The O-atom peaks of MPHCP remained relatively consistent before and after adsorption, whereas P-MPHCP exhibited conspicuous π - π^* interaction peaks post-adsorption. This observation suggests that P-MPHCP demonstrates enhanced π - π^* interactions attributed to its higher benzene ring content.

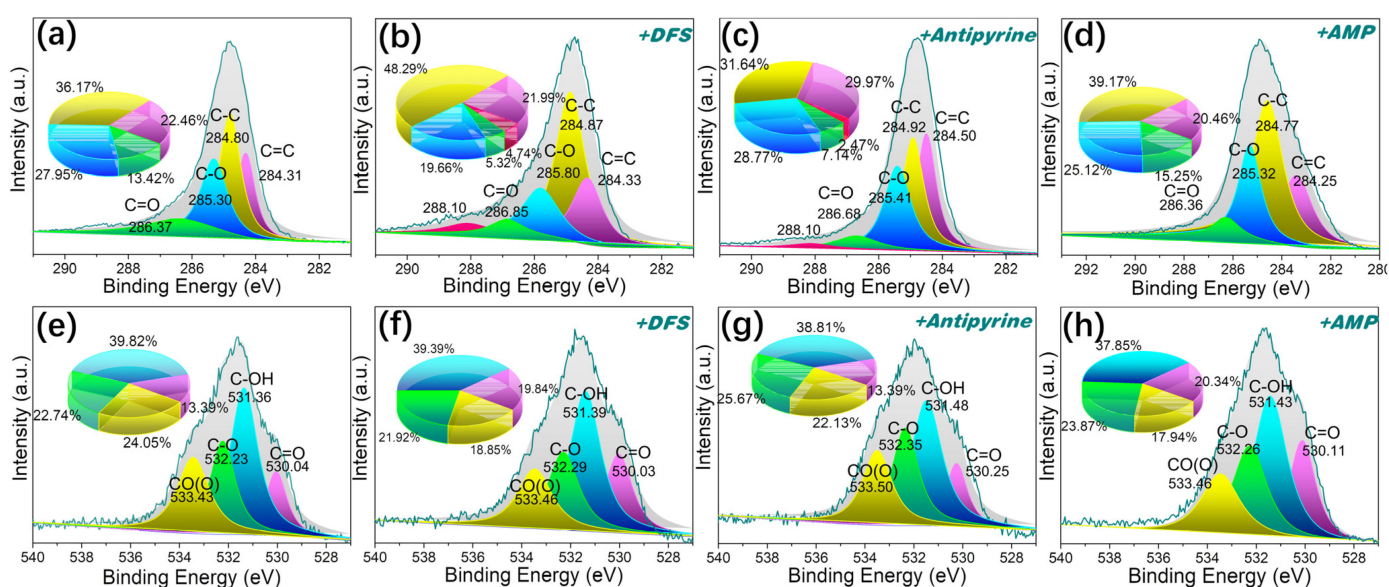


Figure 12. The XPS spectra of C1s (a–d) and O1s (e–h) for P-MPHCP before and after PPCP adsorption.

Therefore, based on the analysis above, the porous structure of the adsorbent shown only provides abundant adsorption sites that, like electrostatic interactions, is not the determining reason for the adsorption capacity. π - π^* interactions and hydrogen bonding are the main mechanisms of adsorption. MPHCP showed evident d-d hydrogen bonding and, after the introduction of a large amount of phenol, the P-MPHCP showed a strong Yoshida-type hydrogen bonding as well as apparent π - π^* interactions.

3. Materials and Methods

3.1. Materials

Ferrosferric oxide (Fe_3O_4 , 50 nm particle size), anhydrous ferric chloride (FeCl_3), 3-phenylglutaric acid, antipyrine, and dimethylformaldehyde (FDA) from Shanghai Aladdin Reagent (Shanghai, China); phenol, 1,2-dichloroethane (DCE), dichloromethane, and anhydrous methanol from Sinopharm Chemical Reagent Company (Shanghai, China); and diclofenac sodium (DFS), 4-acetylaminophenol (AMP), and sodium hydroxide (CaH_2) from Shanghai Sahn Chemical Technology company (Shanghai, China). Before the experiment, the DCE and pitch were dried and dehydrated.

3.2. Preparation of Functionalized Fe₃O₄ Nanoparticles

To prepare the modified magnetic nanoparticles, 20 mL of deionized water and Fe₃O₄ nanoparticles were placed into a flask. The mixture was augmented with 3-phenylglutaric acid and subjected to heating at 80 °C with continuous mechanical stirring for 2 h. Following this, magnetic separation was employed to segregate the solid and liquid phases, with the supernatant subsequently discarded. The solid residue underwent a thorough triple wash with deionized water prior to final drying under vacuum conditions. The final product was named Fe₃O₄@3-phenylglutaric acid NPs. The synthesis process is shown in Figure 1.

3.3. Preparation of Pitch-Based HCPs

In the process of synthesizing the pitch-based HCPs, 0.608 g of pitch was introduced into 40 mL of 1,2-dichloroethane, acting as the monomer. This mixture was subjected to sonication at room temperature until complete dissolution was achieved. Under a nitrogen atmosphere, 0.912 g of dimethylformaldehyde (external crosslinker) and 2.592 g of anhydrous iron (III) chloride (Lewis acid) were introduced and stirred at 80 °C for 24 h. The resulting products were subjected to filtration through anhydrous methanol. Subsequently, further purification was carried out using a Soxhlet extractor for 12 h, employing anhydrous methanol and methylene chloride. Finally, the products underwent a 24 h drying process at 80 °C and were then designated as PHCP.

A total of 0.608 g of pitch was introduced into 40 mL of 1,2-dichloroethane and sonicated until the pitch was completely dissolved at room temperature. A total of 0.16 g of Fe₃O₄@3-phenylglutaric acid NPs were added to the mixture and dispersed evenly. A total of 0.912 g of dimethylformaldehyde and 2.592 g of anhydrous iron (III) chloride as a catalyzer were added to the mixture in a nitrogen atmosphere. The following steps were the same as the preparation of PHCP, the adsorbent powder obtained was named MPHCP.

To synthesize P-MPHCP, we combined 0.608 g of pitch with 40 mL of 1,2-dichloroethane along with 0.16 g of Fe₃O₄@3-phenylglutaric acid NPs and 0.0608 g of phenol, 0.912 g of dimethylformaldehyde, and 2.592 g of anhydrous iron(III) chloride as a Lewis acid, all in a nitrogen atmosphere. The ensuing steps closely mirrored those used for PHCP preparation, ultimately yielding the adsorbent powder known as P-MPHCP. Figure 1 shows the synthetic pathways for three pitch-based HCP adsorbents.

3.4. Characterizations

The methodology and equipment used for characterization, such as Fourier transform infrared spectroscopy (FT-IR, Platinum Elmer, USA), thermogravimetric analysis (TGA, STA449F3 Thermogravimetric instrument, NETZSCH, Germany), X-ray diffraction patterns (XRD, Brock D8 ADVANCE, Brock, Switzerland), a scanning electron microscope (SEM, Su8100 scanning electron microscope, Hitachi, Japan), a high-resolution transmission electron microscope (HRTEM, JEM-2100 F high-resolution transmission electron microscope, JEOL, Japan), Brunauer-Emmett-Teller analysis (BET, ASAP 2020 surface area and porosity analyzer, Micromeritics, USA), X-ray photoelectron spectrometry (XPS, K-alpha device, Thermo Field), and Bruker 400M NMR carbon spectrum (¹³C NMR, Brock, Germany) analysis, were consistent with our previous work [30]. The structural analysis of modified magnetic nanoparticles (FT-IR, TGA, XRD, and SEM) and pitch-based adsorbents (FT-IR, TGA, XRD, SEM, TEM, VSM, and BET) were presented in detail [30].

3.5. Adsorption Experiments

Batch experiments were employed to investigate the adsorption of PPCPs from aqueous solutions. These experiments involved varying process parameters, including pH levels (ranging from 4 to 10), the initial concentration of PPCPs (ranging from 100 to 350 mg L⁻¹), and contact time (ranging from 2 to 360 min). Equilibrium adsorption experiments were performed as follows. Pitch-based HCP adsorbents (5 mg) were administered in 5 mL of DFS, AMP, and antipyrine solutions at concentrations ranging from 100 to 350 mg L⁻¹. Subsequently, the mixture was placed on a temperature-controlled shaker for 6 h to ensure

equilibrium. Thereafter, the adsorbents were separated directly from the solutions through external magnets and the remaining concentrations of PPCPs were determined using a UV-VIS spectrophotometer (TU-1910, Beijing Pu-Analysis, Beijing, China). The adsorption capacity and absorbance of the adsorbent onto the PPCPs were calculated according to Equations (10) and (11) as follows:

$$q_e = \frac{(C_0 - C_e)V}{m} \quad (10)$$

$$U = \frac{C_0 - C_e}{C_0} \times 100\% \quad (11)$$

Within these parameters, C_0 (mg L^{-1}) signifies the initial concentration, q_e (mg g^{-1}) represents the equilibrium adsorption capacity, V (L) denotes the solution volume, m (g) indicates the mass of the adsorbent, U (%) characterizes the adsorption efficiency, and C_e (mg L^{-1}) stands for the equilibrium concentration of the PPCPs.

Kinetic experiments were conducted under optimal pH conditions. Each of the pitch-based HCP adsorbents (50 mg) was added to a 50 mL solution of PPCPs at a concentration of 200 mg L^{-1} at 25°C . Solution samples were harvested at different times (2, 4, 8, 12, 20, 30, 45, 60, 120, 180, 240, and 360 min) and the residual concentration of PPCPs was quantified using UV-VIS spectrophotometry. The adsorption capacity of PPCPs onto each adsorbent at time t (q_t) was calculated using Equation (10) where C_t , the concentration at each sampling time, is substituted for C_e .

The solution pH levels was modulated within the range of 4 to 10 by introducing either 0.1 M NaOH or 0.1 M HCl solution to the PPCP solution. Five mg of adsorbent was added to 5 mL of PPCP solution with different pH values (100 mg L^{-1}) and adsorbed at 25°C for 6 h. The residual concentration of PPCPs was measured to evaluate adsorption capacity.

Thermodynamic experiments were carried out at modified temperatures of 35 and 45°C , with all other conditions remaining the same as the equilibrium experiments. After 6 h of time for the reaction, the remaining concentration of PPCPs was measured to determine the thermodynamic behavior of the adsorbents.

The performance and stability of the adsorbent were evaluated through repeated cycling experiments. The experiments were conducted at an optimal pH level and a PPCP concentration of 200 mg L^{-1} . The adsorbent underwent regeneration using ethanol, which acted as a counter-extraction solution to release the adsorbed PPCPs. The residual PPCPs on the surface of the adsorbent were washed with deionized water, and the adsorbent was ultimately dried. To understand the adsorption rate of PPCPs, the desorption-treated adsorbent was exposed to another 200 mg L^{-1} PPCP solution for further adsorption.

4. Conclusions

Pitch-based HCP adsorbents (PHCP, M-PHCP, and P-MPHCP) were synthesized through the Friedel-Crafts alkylation method and used for the adsorption of PPCPs. For P-MPHCP, according to the Langmuir model fitting parameters, the maximum adsorption capacities of DFS, AMP, and antipyrine were 444.93, 180.89, and 223.62 mg g^{-1} , respectively. Moreover, the thermodynamic study showed that the adsorption of pitch-based adsorbents onto PPCPs was a spontaneous exothermic process. Moreover, even after 5 adsorption-desorption cycles, the adsorption capacity remained nearly unchanged, demonstrating consistently high performance. This resilience was consistently maintained even throughout 10 adsorption-desorption cycles. The porous structure of the adsorbents only provides abundant adsorption sites that, like electrostatic interaction, is not the determining reason for the adsorption capacity. π - π^* interactions and hydrogen bonding are the main mechanisms of adsorption. This study provides technical feasibility for the field of removing PPCPs; the low-cost pitch-based HCP has great potential practical application prospect.

Supplementary Materials: The following supporting information can be downloaded at: <https://www.mdpi.com/article/10.3390/molecules29020463/s1>. Figure S1: Standard curves of DFS (a,d), AMP (b,e), and antipyrine (c,f). Figure S2: Isotherm adsorption capacity for pitch-based HCP adsorbents onto PPCPs (a) DFS, (b) AMP, and (c) antipyrine with different initial concentrations at 35 °C. Figure S3: Isotherm adsorption capacity for pitch-based HCP adsorbents onto PPCPs (a) DFS, (b) AMP, and (c) antipyrine with different initial concentrations at 45 °C. Figure S4: Langmuir (a–c), Freundlich (d–f), and D–R (g–i) isotherms for the adsorption of pitch-based HCP adsorbents onto DFS, AMP, and antipyrine at 35 °C. Figure S5: Langmuir (a–c), Freundlich (d–f), and D–R (g–i) isotherms for the adsorption of pitch-based HCP adsorbents onto DFS, AMP, and antipyrine at 45 °C. Table S1: Correlation coefficient and isotherm parameters for the adsorption of pitch-based HCP adsorbents at 35 °C. Table S2: Correlation coefficient and isotherm parameters for the adsorption of pitch-based HCP adsorbents at 45 °C. Table S3: DFS adsorption performance of P-MPHCP compared with other reported adsorbents. Figure S6: Chemical and structural characteristics of three PPCPs. References [22,32,45–48,52,53,61–64] are cited in the supplementary materials.

Author Contributions: Q.Y., formal analysis, data curation, methodology; H.Z., data curation, writing—original draft, investigation, visualization, methodology, conceptualization; Q.P., data curation, formal analysis, methodology; G.C., software, methodology; J.L., methodology; X.C., methodology; S.X., data curation; G.L., formal analysis; Q.L., conceptualization, data curation, project administration, funding acquisition. All authors have read and agreed to the published version of the manuscript.

Funding: This research was funded by the National Natural Science Foundation of China (Grant No. 51778226, 22008060) and the Hunan Provincial Natural Science Foundation, China (Grant No. 2023JJ30227).

Institutional Review Board Statement: Not applicable.

Informed Consent Statement: Not applicable.

Data Availability Statement: Data are contained within the article and Supplementary Materials.

Acknowledgments: The authors gratefully acknowledge the National Natural Science Foundation of China and the Hunan Provincial Natural Science Foundation, China.

Conflicts of Interest: The authors declare no conflict of interest.

References

1. Iovino, P.; Lavorgna, M.; Orlo, E.; Russo, C.; Felice, B.D.; Campolattano, N.; Muscariello, L.; Fenti, A.; Chianese, S.; Isidori, M.; et al. An integrated approach for the assessment of the electrochemical oxidation of diclofenac: By-product identification, microbiological and Eco-genotoxicological evaluation. *Sci. Total Environ.* **2024**, *909*, 168511. [[CrossRef](#)] [[PubMed](#)]
2. Gu, J.; Zhang, L.; Wang, X.J.; Lu, C.Y.; Liu, J.Y.; Liu, Y.; Li, L.C.; Peng, J.Y.; Xue, M.M. High-throughput analysis of the effects of different fish culture methods on antibiotic resistance gene abundances in a lake. *Environ. Sci. Pollut. Res.* **2019**, *26*, 5445–5453. [[CrossRef](#)]
3. Gomes, A.L.M.; Andrade, P.H.M.; Palhares, H.G.; Dumont, M.R.; Soares, D.C.F.; Volkringer, C.; Houmard, M.; Nunes, E.H.M. Facile Sol-gel synthesis of silica sorbents for the removal of organic pollutants from aqueous media. *J. Mater. Res. Technol.* **2021**, *15*, 4580–4594. [[CrossRef](#)]
4. Phoon, B.L.; Ong, C.C.; Saheed, M.S.M.; Show, P.-L.; Chang, J.-S.; Ling, T.C.; Lam, S.S.; Juan, J.C. Conventional and emerging technologies for removal of antibiotics from wastewater. *J. Hazard. Mater.* **2020**, *400*, 122961. [[CrossRef](#)] [[PubMed](#)]
5. Gopal, C.M.; Bhat, K.; Praveenkumarreddy, Y.; Shailesh; Kumar, V.; Basu, H.; Joshua, D.I.; Singhal, R.K.; Balakrishna, K. Evaluation of selected pharmaceuticals and personal care products in water matrix using ion trap mass spectrometry: A simple weighted calibration curve approach. *J. Pharm. Biomed. Anal.* **2020**, *185*, 113214. [[CrossRef](#)] [[PubMed](#)]
6. Vitiello, A.; Zovi, A.; Trama, U.; Ferrara, F. Overview of pharmacotherapy targeting COVID-19 disease based on ACE-2: Current challenges and future directions. *Herz* **2023**, *48*, 372–375. [[CrossRef](#)] [[PubMed](#)]
7. Villa, S.; Nica, V.D.; Castiglioni, S.; Finizio, A. Environmental risk classification of emerging contaminants in an alpine stream influenced by seasonal tourism. *Ecol. Indic.* **2020**, *115*, 106428. [[CrossRef](#)]
8. Manikandan, S.K.; Pallavi, P.; Shetty, K.; Bhattacharjee, D.; Giannakoudakis, D.A.; Katsoyiannis, I.A.; Nair, V. Effective usage of biochar and microorganisms for the removal of heavy metal ions and pesticides. *Molecules* **2023**, *28*, 719. [[CrossRef](#)]
9. Liu, J.-L.; Wong, M.-H. Pharmaceuticals and personal care products (PPCPs): A review on environmental contamination in China. *Environ. Int.* **2013**, *59*, 208–224. [[CrossRef](#)]
10. Patel, M.; Kumar, R.; Kishor, K.; Mlsna, T.; Pittman, C.U., Jr.; Mohan, D. Pharmaceuticals of emerging concern in aquatic systems: Chemistry, occurrence, effects, and removal methods. *Chem. Rev.* **2019**, *119*, 3510–3673. [[CrossRef](#)]

11. Blair, B.; Nikolaus, A.; Hedman, C.; Klaper, R.; Grundl, T. Evaluating the degradation, sorption, and negative mass balances of pharmaceuticals and personal care products during wastewater treatment. *Chemosphere* **2015**, *134*, 395–401. [[CrossRef](#)] [[PubMed](#)]
12. Gao, P.; Ding, Y.J.; Li, H.; Xagorarakis, I. Occurrence of pharmaceuticals in a municipal wastewater treatment plant: Mass balance and removal processes. *Chemosphere* **2012**, *88*, 17–24. [[CrossRef](#)] [[PubMed](#)]
13. Baig, U.; Waheed, A.; Aljundi, I.H.; AbuMousa, R.A. Facile fabrication of graphitic carbon nitride nanosheets and its integrated polyamide Hyper-cross-linked TFC nanofiltration membrane with intrinsicmolecular porosity for salts and organic pollutant rejection from water. *J. Mater. Res. Technol.* **2021**, *15*, 6319–6328. [[CrossRef](#)]
14. Wang, Y.F.; Huang, H.O.; Wei, X.M. Influence of wastewater pre-coagulation on adsorptive filtration of pharmaceutical and personal care products by carbon nanotube membranes. *Chem. Eng. J.* **2018**, *333*, 66–75. [[CrossRef](#)]
15. Chianese, S.; Fenti, A.; Blotvogel, J.; Musmarra, D.; Iovino, P. Trimethoprim removal from wastewater: Adsorption and Electro-oxidation comparative case study. *Case Stud. Chem. Environ. Eng.* **2023**, *8*, 100433. [[CrossRef](#)]
16. Zheng, X.S.; Wang, Z.Q.; Chen, T.S.; Ran, J.; Wu, Y.L.; Tan, C.W.; Zhang, Q.X.; Chen, P.; Wang, F.L.; Liu, H.J.; et al. One-step synthesis of carbon nitride nanobelts for the enhanced photocatalytic degradation of organic pollutants through peroxydisulfate activation. *Environ. Sci. Nano* **2021**, *8*, 245–257. [[CrossRef](#)]
17. Eniola, J.O.; Kumar, R.; Barakat, M.A.; Rashid, J. A review on conventional and advanced hybrid technologies for pharmaceutical wastewater treatment. *J. Clean. Prod.* **2022**, *356*, 131826. [[CrossRef](#)]
18. Yang, R.T. *Adsorbents: Fundamentals and Applications*; John Wiley & Sons: Hoboken, NJ, USA, 2003.
19. Barczak, M.; Pietras-Ozga, D.; Seliem, M.K.; de Falco, G.; Giannakoudakis, D.A.; Triantafyllidis, K. Mesoporous silicas obtained by Time-controlled Co-condensation: A strategy for tuning structure and sorption properties. *Nanomaterials* **2023**, *13*, 2065. [[CrossRef](#)]
20. Arkas, M.; Giannakopoulos, K.; Favvas, E.P.; Papageorgiou, S.; Theodorakopoulos, G.V.; Giannoulitou, A.; Vardavoulias, M.; Giannakoudakis, D.A.; Triantafyllidis, K.S.; Georgiou, E.; et al. Comparative study of the U(VI) adsorption by hybrid Silica-hyperbranched poly(ethylene imine) nanoparticles and xerogels. *Nanomaterials* **2023**, *13*, 1794. [[CrossRef](#)]
21. Peng, Q.; Zhao, H.W.; Wang, R.Y.; Cao, X.X.; Liu, H.; Liu, Q.Q. Ferrocene-based hypercrosslinked polymers derived from phenolic polycondensation with unexpected H₂ adsorption capacity. *Mater. Today Chem.* **2022**, *24*, 100854. [[CrossRef](#)]
22. Ravi, S.; Choi, Y.J.; Choe, J.K. Novel Phenyl-phosphate-based porous organic polymers for removal of pharmaceutical contaminants in water. *Chem. Eng. J.* **2020**, *379*, 122290. [[CrossRef](#)]
23. Gan, Y.Q.; Chen, G.; Sang, Y.F.; Zhou, F.; Man, R.L.; Huang, J.H. Oxygen-rich Hyper-cross-linked polymers with hierarchical porosity for aniline adsorption. *Chem. Eng. J.* **2019**, *368*, 29–36. [[CrossRef](#)]
24. Hao, J.; Zhang, Q.X.; Chen, P.; Zheng, X.S.; Wu, Y.L.; Ma, D.; Wei, D.D.; Liu, H.J.; Liu, G.G.; Lv, W.Y. Removal of pharmaceuticals and personal care products (PPCPs) from water and wastewater using novel sulfonic acid (-SO₃H) functionalized covalent organic frameworks. *Environ. Sci. Nano* **2019**, *6*, 3374. [[CrossRef](#)]
25. Li, W.Q.; Zhang, A.J.; Gao, H.; Chen, M.J.; Liu, A.H.; Bai, H.; Li, L. Massive preparation of Pitch-based organic microporous polymers for gas storage. *Chem. Commun.* **2016**, *52*, 2780–2783. [[CrossRef](#)] [[PubMed](#)]
26. Yang, Y.; He, Z.P.; Liu, Y.; Wang, S.L.; Wang, H.G.; Zhu, G.S. Facile preparation of N-doped hierarchically porous carbon derived from Pitch-based Hyper-cross-linked polymers as an efficient Metal-free catalyst for Oxygen-reduction. *Appl. Surf. Sci.* **2021**, *565*, 150579. [[CrossRef](#)]
27. Dharmaratne, N.U.; Jouaneh, T.M.M.; Kiesewetter, M.K.; Mathers, R.T. Quantitative measurements of polymer hydrophobicity based on functional group identity and oligomer length. *Macromolecules* **2018**, *51*, 8461–8468. [[CrossRef](#)]
28. Tang, Z.H.; He, C.L.; Tian, H.Y.; Ding, J.X.; Hsiao, B.S.; Chu, B.; Chen, X.S. Polymeric nanostructured materials for biomedical applications. *Prog. Polym. Sci.* **2016**, *60*, 86–128. [[CrossRef](#)]
29. Sato, K.; Oaki, Y.; Imai, H. A hydrophobic adsorbent based on hierarchical porous polymers derived from morphologies of a biomineral. *Chem. Commun.* **2015**, *51*, 7919–7922. [[CrossRef](#)]
30. Peng, Q.; Zhao, H.W.; Chen, G.; Yang, Q.L.; Cao, X.X.; Xiong, S.H.; Xiao, A.G.; Li, G.; Liu, B.; Liu, Q.Q. Synthesis of novel magnetic Pitch-based hypercrosslinked polymers as adsorbents for effective recovery of Ag⁺ with high selectivity. *J. Environ. Manag.* **2023**, *339*, 117763. [[CrossRef](#)]
31. Bautista-Toledo, I.; Ferro-García, M.A.; Rivera-Utrilla, J.; Moreno-Castilla, C.; Fernández, F.J.V. Bisphenol a removal from water by activated carbon. Effects of carbon characteristics and solution chemistry. *Environ. Sci. Technol.* **2005**, *39*, 6246–6250. [[CrossRef](#)]
32. Mi, X.; Zhou, S.X.; Zhou, Z.M.; Vakili, M.; Qi, Y.; Jia, Y.; Zhu, D.H.; Wang, W. Adsorptive removal of diclofenac sodium from aqueous solution by magnetic COF: Role of hydroxyl group on COF. *Colloids Surf. A Physicochem. Eng. Asp.* **2022**, *603*, 125238. [[CrossRef](#)]
33. Lagergren, S. Zur theorie der sogenannten adsorption gelöster stoffe. *K. Sven. Vetenskapsakademiens Handl.* **1898**, *24*, 1–39.
34. Ho, Y.S.; McKay, G. Pseudo-second order model for sorption processes. *Process Biochem.* **1999**, *34*, 451–465. [[CrossRef](#)]
35. Nestic, A.R.; Velickovic, S.J.; Antonovic, D.G. Novel composite films based on amidated pectin for cationic dye adsorption. *Colloids Surf. B Biointerfaces* **2014**, *116*, 620–626. [[CrossRef](#)] [[PubMed](#)]
36. Zhang, W.; Song, J.Y.; He, Q.L.; Wang, H.Y.; Lyu, W.L.; Feng, H.J.; Xiong, W.Q.; Guo, W.B.; Wu, J.; Chen, L. Novel pectin based composite hydrogel derived from grapefruit peel for enhanced Cu(II) removal. *J. Hazard. Mater.* **2020**, *384*, 121445. [[CrossRef](#)] [[PubMed](#)]
37. Langmuir, I. The constitution and fundamental properties of solids and liquids part I solids. *J. Am. Chem. Soc.* **1916**, *38*, 2221–2295. [[CrossRef](#)]

38. Freundlich, H.M.F. Über die adsorption in lösungen. *Z. Phys. Chem. A* **1906**, *57*, 385–470. [[CrossRef](#)]
39. Hutson, N.D.; Yang, R.T. Theoretical basis for the Dubinin-radushkevitch (D-R) adsorption isotherm equation. *Adsorption* **1997**, *3*, 189–195. [[CrossRef](#)]
40. Li, Z.Y.; Liu, X.R.; Zhang, X.; Zhang, T.Y.; Chen, J.; Li, Q.; Yu, Y.C.; Zhao, X.Y.; Wei, Y. Fabrication of Hydroxyl-carboxyl bifunctional Hyper-crosslinked polymers for selective adsorption of methylene blue. *Chem. Eng. Technol.* **2022**, *45*, 2178–2185. [[CrossRef](#)]
41. Savić, J.Z.; Vasić, V.M. Thermodynamics and kinetics of 1,8-dihydroxy-2-(imidazol-5-ylazo)-naphthalene-3,6-disulphonic acid immobilization on dowex resin. *Colloids Surf. A Physicochem. Eng. Asp.* **2006**, *278*, 197–203. [[CrossRef](#)]
42. Pan, B.J.; Pan, B.C.; Zhang, W.M.; Zhang, Q.R.; Zhang, Q.X.; Zheng, S.R. Adsorptive removal of phenol from aqueous phase by using a porous acrylic ester polymer. *J. Hazard. Mater.* **2008**, *157*, 293–299. [[CrossRef](#)] [[PubMed](#)]
43. Uzun, İ.; Güzel, F. Kinetics and thermodynamics of the adsorption of some dyestuffs and P-nitrophenol by chitosan and MCM-chitosan from aqueous solution. *J. Colloid Interface Sci.* **2004**, *274*, 398–412. [[CrossRef](#)] [[PubMed](#)]
44. Barczak, M.; Dobrowolski, R.; Borowski, P.; Giannakoudakis, D.A. Pyridine-, thiol- and amine-functionalized mesoporous silicas for adsorptive removal of pharmaceuticals. *Microporous Mesoporous Mater.* **2022**, *299*, 110132. [[CrossRef](#)]
45. Bhadra, B.N.; Seo, P.W.; Jhung, S.H. Adsorption of diclofenac sodium from water using oxidized activated carbon. *Chem. Eng. J.* **2016**, *301*, 27–34. [[CrossRef](#)]
46. Bhadra, B.N.; Ahmed, I.; Kim, S.; Jhung, S.H. Adsorptive removal of ibuprofen and diclofenac from water using metal-organic framework-derived porous carbon. *Chem. Eng. J.* **2017**, *314*, 50–58. [[CrossRef](#)]
47. Andrew Lin, K.Y.; Yang, H.; Lee, W.D. Enhanced removal of diclofenac from water using a zeolitic imidazole framework functionalized with cetyltrimethylammonium bromide (CTAB). *RSC Adv.* **2015**, *5*, 81330–81340. [[CrossRef](#)]
48. Zheng, X.; Wang, J.L.; Xue, X.L.; Liu, W.X.; Kong, Y.D.; Cheng, R.; Yuan, D.H. Facile synthesis of Fe₃O₄@MOF-100(Fe) magnetic microspheres for the adsorption of diclofenac sodium in aqueous solution. *Environ. Sci. Pollut. Res.* **2018**, *25*, 31705–31717. [[CrossRef](#)] [[PubMed](#)]
49. Ouyang, J.B.; Zhou, L.M.; Liu, Z.R.; Heng, J.Y.Y.; Chen, W.Q. Biomass-derived activated carbons for the removal of pharmaceutical micropollutants from wastewater: A review. *Sep. Purif. Technol.* **2020**, *253*, 117536. [[CrossRef](#)]
50. Paunovic, O.; Pap, S.; Maletic, S.; Taggart, M.A.; Boskovic, N.; Sekulic, M.T. Ionisable emerging pharmaceutical adsorption onto microwave functionalised biochar derived from novel lignocellulosic waste biomass. *J. Colloid Interface Sci.* **2019**, *547*, 350–360. [[CrossRef](#)]
51. Baccar, R.; Sarrà, M.; Bouzid, J.; Feki, M.; Blánquez, P. Removal of pharmaceutical compounds by activated carbon prepared from agricultural By-product. *Chem. Eng. J.* **2012**, *211–212*, 310–317. [[CrossRef](#)]
52. Sangster, J. Phase Diagrams and Thermodynamic Properties of Binary Organic Systems Based on 1,2-, 1,3-, 1,4-Diaminobenzene or Benzidine. *J. Phys. Chem. Ref. Data* **1994**, *23*, 295–338. [[CrossRef](#)]
53. Mark, F.H.; Jennifer, L.L. Determination of logKow Values for Four Drugs. *J. Chem. Educ.* **2014**, *91*, 915–918.
54. Lee, S.; Kim, Y.; Choi, P.J.; Jang, A. Predicting the removal efficiency of pharmaceutical and personal care products using heated metal oxides as adsorbents based on their physicochemical characteristics. *Chemosphere* **2023**, *339*, 139665. [[CrossRef](#)] [[PubMed](#)]
55. Tran, H.N.; Wang, Y.-F.; You, S.-J.; Chao, H.-P. Insights into the mechanism of cationic dye adsorption on activated charcoal: The importance of π - π interactions. *Process Saf. Environ. Prot.* **2017**, *107*, 168–180. [[CrossRef](#)]
56. Lladó, J.; Lao-Luque, C.; Ruiz, B.; Fuente, E.; Solé-Sardans, M.; Dorado, A.D. Role of activated carbon properties in atrazine and paracetamol adsorption equilibrium and kinetics. *Process Saf. Environ. Prot.* **2015**, *95*, 51–59. [[CrossRef](#)]
57. Wang, M.Q.; Wang, C.Y.; Song, Y.J.; Zhang, C.H.; Shao, L.; Jiang, Z.X.; Huang, Y.D. Facile method to functionalize graphene oxide nanoribbons and its application to poly(p-phenylene benzobisoxazole) composite. *Compos. Sci. Technol.* **2018**, *165*, 124–130. [[CrossRef](#)]
58. Ortiz-Martínez, K.; Guerrero-Medina, K.J.; Román, F.R.; Hernández-Maldonado, A.J. Transition metal modified mesoporous silica adsorbents with zero microporosity for the adsorption of contaminants of emerging concern (CECs) from aqueous solutions. *Chem. Eng. J.* **2015**, *264*, 152–164. [[CrossRef](#)]
59. Pan, N.; Li, L.; Ding, J.; Wang, R.B.; Jin, Y.D.; Xia, C.Q. A Schiff base/quaternary ammonium salt bifunctional graphene oxide as an efficient adsorbent for removal of Th(IV)/U(VI). *J. Colloid Interface Sci.* **2017**, *508*, 303–312. [[CrossRef](#)]
60. Duguet, T.; Gavrielides, A.; Esvan, J.; Mineva, T.; Lacaze-Dufaure, C. DFT Simulation of XPS reveals Cu/Epoxy polymer interfacial bonding. *J. Phys. Chem. C* **2019**, *123*, 30917–30925. [[CrossRef](#)]
61. Vedenyapina, M.D.; Borisova, D.A.; Simakova, A.P.; Proshina, L.P.; Vedenyapin, A.A. Adsorption of diclofenac sodium from aqueous solutions on expanded graphite. *Solid Fuel Chem.* **2013**, *47*, 59–63. [[CrossRef](#)]
62. Ravi, S.; Choi, Y.; Wu, S.; Xiao, R.; Bae, Y.S. Porous organic nanofiber polymers as superfast adsorbents for capturing pharmaceutical contaminants from water. *Environ. Sci. Nano* **2022**, *9*, 730–741. [[CrossRef](#)]
63. Krajišnik, D.; Daković, A.; Milojević, M.; Malenović, A.; Kragović, M.; Bogdanović, D.B.; Dondur, V.; Milić, J. Properties of diclofenac sodium sorption onto natural zeolite modified with cetylpyridinium chloride. *Colloids Surf. B Biointerfaces* **2011**, *83*, 165–172. [[CrossRef](#)] [[PubMed](#)]
64. Wei, H.; Deng, S.; Huang, Q.; Nie, Y.; Wang, B.; Huang, J.; Yu, G. Regenerable granular carbon nanotubes/alumina hybrid adsorbents for diclofenac sodium and carbamazepine removal from aqueous solution. *Water Res.* **2013**, *47*, 4139–4147. [[CrossRef](#)] [[PubMed](#)]

Disclaimer/Publisher’s Note: The statements, opinions and data contained in all publications are solely those of the individual author(s) and contributor(s) and not of MDPI and/or the editor(s). MDPI and/or the editor(s) disclaim responsibility for any injury to people or property resulting from any ideas, methods, instructions or products referred to in the content.